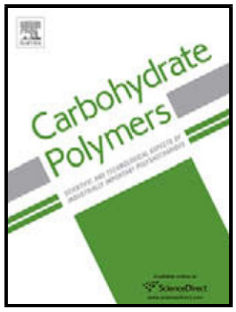


Title: Scaffolds based on alginate-PEG methyl ether methacrylate-*Moringa oleifera-Aloe vera* for wound healing applications

Authors: Itzel Rubio-Elizalde, Johanna Bernáldez-Sarabia, Aldo Moreno-Ulloa, Carmel Vilanova, Patricia Juárez, Alexei Licea-Navarro, Ana B. Castro-Ceseña

PII: S0144-8617(18)31360-2
DOI: https://doi.org/10.1016/j.carbpol.2018.11.027
Reference: CARP 14278

To appear in:

Received date: 20 July 2018
Revised date: 8 November 2018
Accepted date: 8 November 2018

Please cite this article as: Rubio-Elizalde I, Bernáldez-Sarabia J, Moreno-Ulloa A, Vilanova C, Juárez P, Licea-Navarro A, Castro-Ceseña AB, Scaffolds based on alginate-PEG methyl ether methacrylate-*Moringa oleifera-Aloe vera* for wound healing applications, *Carbohydrate Polymers* (2018), https://doi.org/10.1016/j.carbpol.2018.11.027

# Scaffolds based on alginate-PEG methyl ether methacrylate-*Moringa oleifera*-*Aloe vera* for wound healing applications

Itzel Rubio-Elizalde[a,b], Johanna Bernáldez-Sarabia[b], Aldo Moreno-Ulloa[b], Carmel Vilanova[b], Patricia Juárez[b], Alexei Licea-Navarro[b], Ana B. Castro-Ceseña[b,c]*

[a]*Universidad Nacional Autónoma de México (UNAM), Carretera Tijuana-Ensenada, Apdo. Postal, 356, C.P. 22800, Ensenada, Baja California, México.*
[b]*Departamento de Innovación Biomédica, Centro de Investigación Científica y de Educación Superior de Ensenada (CICESE), Carretera Ensenada-Tijuana No. 3918, Zona Playitas, C.P. 22860, Ensenada, Baja California, México*
[c]*CONACyT-Centro de Investigación y Desarrollo Tecnológico en Electroquímica (CIDETEQ), Parque Tecnológico Querétaro – Sanfandila, C.P. 76703, Pedro Escobedo, Querétaro, México*

*Corresponding author:
Ana B. Castro-Ceseña: acastro@cicese.mx
Tel.: +52 646 175 0500, Ext.: 27271

Graphical abstract

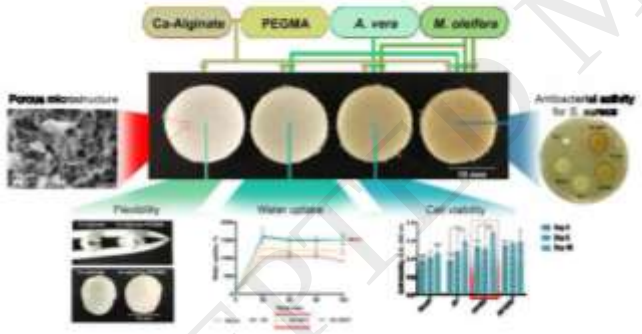


## Highlights

1. PEGMA, as plasticizer, improves stability properties of alginate-based scaffolds
2. Alginate-PEGMA-*A. vera*-*M. oleifera* scaffolds with wound healing promotion features
3. Alginate-PEGMA scaffolds with *M. oleifera* inhibit the proliferation of *S. aureus*
4. Viability of skin fibroblasts increases in scaffolds with *A. vera* and *M. oleifera*

## Abstract

This study sought to improve the handling, stability to aqueous medium and healing properties of alginate-based three-dimensional structures to be applied as wound scaffolds. Thus, Ca-alginate was plasticized with PEG-methyl ether methacrylate (PEGMA) and blended with the freeze-dried gel of *A. vera* and aqueous leaves extracts of *M. oleifera*. Ca-alginate-PEGMA scaffolds remained structurally stable almost four times longer than pure alginate materials, while a high porous architecture required for tissue scaffolding applications was maintained after alginate plasticization with PEGMA. *A. vera* increased the water uptake capability of the scaffolds and *M. oleifera* provided antioxidant capacity, anti-inflammatory properties and antimicrobial activity against *S. aureus*. Blending 1% (w/v) *A. vera* and 1% (w/v) *M. oleifera* with Ca-alginate-PEGMA, significantly increased the scaffolds cell viability (after 10 days of evaluation), compared with scaffolds without plant extracts. The experimental results showed that Ca-alginate-PEGMA/*A. vera*/*M. oleifera* biocomposites have great potential for wound healing applications.

Keywords: alginate; plasticization; scaffolds; wound healing; *Moringa oleifera*; *Aloe vera*.

## 1. Introduction

Wound healing *per se* is a complex process that involves a well-orchestrated integration of biological and molecular events such as cell migration, cell proliferation, and extracellular matrix deposition (Falanga, 2005). Scaffolds, as three-dimensional structures, that not only provide support for tissue formation, but also can cover a wound and be a physical barrier against external infection (Zhong, Zhang & Lim, 2010), are an alternative to facilitate wound healing (Chanda et al., 2018; Guo et al., 2018; Kumar Ramadass, et al., 2014. With respect to their properties, scaffolds must be porous and biocompatible because cells need to adhere and migrate through these three dimensional networks. Scaffolds also need to be biodegradable to allow cells to produce their own extracellular matrix (O'Brien, 2011). These structural and functional characteristics should be consider when designing a scaffold for wound healing applications, while keeping its fabrication cost effective and possible to scale-up from making one at time in the research laboratory to small batch production (Partap, Lyons & O'Brien, 2010). Based on these requirements, polysaccharides are promising candidates for wound care and tissue engineering. Alginate as one of such polysaccharides, is intrinsically biocompatible, biodegradable and is readily available. It consists of two guluronic acid (G) and two mannuronic acid (M) residues with (1,4)-linkages (Augst, Kong & Mooney, 2006). When calcium ions ($Ca^{2+}$) are added, an "egg-box" structure is formed under the cation interaction between $Ca^{2+}$ and the guluronate blocks of alginate (Cheng et al., 2017; Pereira, Carvalho, Gil, Mendes & Bártolo, 2013), this makes processing of alginate cost effective. Moreover, alginate-based materials have been previously used for wound healing applications due to their hemostatic properties (Catanzano, D'Esposito, Formisano, Boateng & Quaglia, 2018; Cheng et al., 2017). However, for tissue scaffolding applications, pure alginate materials have poor structural integrity, thus inadequate handling and stability properties (Stagnaro, Schizzi, Utzeri, Marsano & Castellano, 2018). To overcome this drawback, plasticization, which reduces the intermolecular attraction forces between polymers chains (Ranjan Saha et al., 2018), may increase the handling and stability of the alginate-based materials. However, the alginate:plasticizer ratio should be fine-

tuned in order to improve the handling and stability properties, while keeping the porous architecture required for materials for tissue scaffolding applications.

While scaffolds facilitate regeneration of a wounded tissue, since they act as templates for tissue formation, it is also likely that incorporation of natural compounds with wound healing effects, such as antioxidant, anti-inflammatory and antimicrobial properties, will thus produce an advanced dressing for wound healing applications. Flowering plants like *Aloe vera* (*A. vera*) and *Moringa oleifera* (*M. oleifera*) contain phytochemical compounds that promote wound healing given their antioxidant, antimicrobial and anti-inflammatory properties (Shah & Amini-Nik, 2017). The clear mucilaginous gel of *A. vera*, obtained from the leaf pulp, has been reported to have physiologically active compounds that accelerate wound healing and promote the rate of wound closure (Li et al., 2017). A study regarding the evaluation of aqueous leaves extracts of *M. oleifera*, for wound healing in albino rats model, showed that wounds closed faster than those without treatment (Rathi, Bodhankar & Baheti, 2006). Moreover, the organic active components in the gel of *A. vera* increase fibroblasts adhesion and proliferation (Li et al., 2017), and aqueous leaves extracts of *M. oleifera* promote proliferation of human dermal fibroblasts cells (Chin, Jalil, Ng & Ng, 2018). These characteristics are of particular interest, since alginate structure lacks signal sequence for cell adhesion (Sun & Tan, 2013). Based on this, we hypothesize that incorporation of *A. vera* and *M. oleifera* will increase the cell proliferation through the alginate scaffolds, and provide wound healing properties via the biological effects associated with the polyphenol content of these plants. While incorporation of a plasticizer, such as poly(ethylene glycol) methyl ether methacrylate (PEGMA), in the optimum ratio will improve the handling and stability to aqueous medium properties of the scaffolds without compromising the porous architecture required for tissue scaffolding applications.

The development of porous dressings incorporating natural wound healing agents, such as honey, as well as extracts from certain plants (*Allium sativum* and *Cleome droserifolia*) have been reported recently (Sarhan, Azzazy & El-Sherbiny, 2016; Sarkar, Ghosh, Barui & Datta, 2018). These studies are more focused on enhancing the antimicrobial properties of the dressing materials (Sarhan & El-Sherbiny, 2016), and on achieving suitable concentrations of the natural healing agents for wound healing support (Sarkar et al., 2018). However, to the best of our knowledge, no work has been conducted on enhancing the handling and stability to aqueous medium properties of scaffolds by incorporating a plasticizer, while at the same time, the porous architecture required for tissue scaffolding applications is maintained. Thus, the present study sought to increase the handling and stability to aqueous medium of alginate-based scaffolds by plasticization with PEGMA, and the cell proliferation and wound healing properties via the biological effects associated with the polyphenol content of *A. vera* and *M. oleifera*. The effect of PEGMA on the chemical properties of the scaffolds are analyzed and compared on the stability to aqueous medium and shape retention properties of these alginate-based materials for wound healing applications. The antioxidant, anti-inflammatory and antimicrobial properties of the obtained scaffolds are evaluated, as well as their effects on cell viability using human skin fibroblasts as an *in vitro* model.

## 2. Materials and methods

### 2.1. Materials

*Aloe vera* (*Aloe barbadensis* Miller) leaves were obtained from a greenhouse in Ecoparque – El Colegio de la Frontera Norte, Tijuana, México, in January 2018. *Moringa oleifera* leaves were bought from *Stevia San Martín* (certified organic by Agricert México) in January 2018. Alginic acid sodium salt with molecular weight of 120,000 – 190,000 g/mol, and a mannuronic acid to guluronic acid ratio (M/G) of 1.56 was purchased from Sigma-Aldrich, México, Cat. No. 180947. As well as poly(ethylene glycol) methyl ether methacrylate, Mn ~500 Da (Cat. No. 447943). Calcium chloride ($CaCl_2$), Folin-Ciocalteu, gallic acid, (±)-6-Hydroxy-2,5,7,8-tetramethylchromane-2-carboxylic acid (Trolox), 2,2-difenil-1-picrilhidrazil (DPPH), sodium nitroprusside (SNP), Griess Reagent, and sodium nitrite ($NaNO_2$) were also purchased from Sigma-Aldrich, México. Human skin fibroblasts CCD-1112Sk (ATCC CRL-2429), *Staphylococcus aureus* (ATCC 25923) and *Escherichia coli* (ATCC 25922) were obtained from the American Type Culture Collection, ATCC.

2.2. Preparation of aqueous extracts

Is been reported that the organic components of the gel of *A. vera* and the aqueous leaves extracts of *M. oleifera* increase adhesion and proliferation of fibroblasts (Chin et al., 2018; Li et al., 2017), which may contribute overcoming the lack of cell adhesion sequences in pure alginate scaffolds. Based on this, *A. vera* gel and aqueous extracts of *M. oleifera* leaves were obtained as follows: *A*. *vera* leaves were left to drain overnight at 4°C to remove the yellowish latex. A colorless liquid from *A. vera* gel leaves was collected, frozen at -80°C, and freeze-dried. Dry *M. oleifera* leaves were pulverized and used for an aqueous extraction at 75°C for 5 min and filtered using a 0.2 µm filter. *M. oleifera* extract was frozen at -80°C and freeze-dried (**Fig. 1a**). Freeze-dried extracts were stored at 4°C until use. Since the obtained extracts were completely water-soluble, a homogeneous distribution of the plant extracts through the scaffolds was achieved, by the procedure described next.

2.3. Preparation of the composite scaffolds

The scaffolds were prepared as follows: PEGMA was added to a sodium alginate solution to final concentrations of 0.375% (v/v) and 1.5% (w/v), respectively, and homogenized using a stick blender. The alginate was crosslinked with $Ca^{2+}$ by adding an equal volume of $CaCl_2$ to a final concentration of 0.75% (w/v), while stirring intensively with the stick blender, until a smooth solution was obtained (Shapiro & Cohen, 1997; Zmora, Glicklis, Cohen, 2002). In order to determine the concentration of *M. oleifera*, we evaluated 1, 2, and 3% (w/v) solutions in 6 mm Whatman® disks, by the agar disk diffusion method, using Carbenicillin® (30 µl of a 500 µg/ml solution) as control. The three concentrations showed antimicrobial activity against *S. aureus*, and the diameter of the inhibition zone increased as the concentration of *M. oleifera* was higher. In particular, the diameter of the inhibition zone of the 1% (w/v) *M. oleifera* solution, was similar to that of the control (results not shown). Thus, we choose 1% (w/v) *M. oleifera* because of its comparable antimicrobial effect to our control. However, we also decided to prepare and evaluate scaffolds with 2% (w/v) *M. oleifera*, in case we would detect a decreased antimicrobial activity after its blending with the other components to form the scaffolds. *A. vera* did not show antibacterial activity under the experimental conditions of the antimicrobial preliminary assays

(results not presented). However, the *A. vera* gel contains highly hydrophilic compounds, which could increase the cell affinity of the composite scaffolds. Thus, a concentration of 1% (w/v) *A. vera* was chosen based on the maximum concentration of the freeze-dried extract that could allow preservation of the structural integrity of the scaffolds. Given the preliminary results, we were interested in studying the effect of the *A. vera*-*M. oleifera* blend. However, *A. vera* composite scaffolds were also prepared in order to obtain information regarding its effect on water uptake, given the high hydrophilicity of its components. Based on this, freeze-dried *M. oleifera* and/or *A. vera* extracts were added to the resulting Ca-alginate-PEGMA solution at final concentrations of 1% (w/v) *A. vera*, 1%(w/v) *A. vera*-1% (w/v) *M. oleifera* and 1% (w/v) *A. vera*-2% (w/v) *M. oleifera* and designated as AV, AV-MO and AV-2MO, respectively (**Fig. 1b**). Each solution (0.6 ml) was poured onto 24-well plates and frozen for 48 h (**Fig. 1c**), followed by freeze-drying (Labconco FreeZone, 1L) for 24 h (**Fig. 1d**) to form the porous sponges designated as AV, AV-MO and AV-2MO composite scaffolds. All the solutions were prepared in water. Pure alginate scaffolds were prepared following the same method, without the addition of PEGMA for evaluating its interaction with alginate, shape retention and stability behavior. All of the other properties, such as antioxidant, anti-inflammatory, antimicrobial and cell viability, were evaluated using Ca-alginate-PEGMA scaffolds without *M. oleifera* and/or *A. vera* extracts, designated as blank scaffolds.

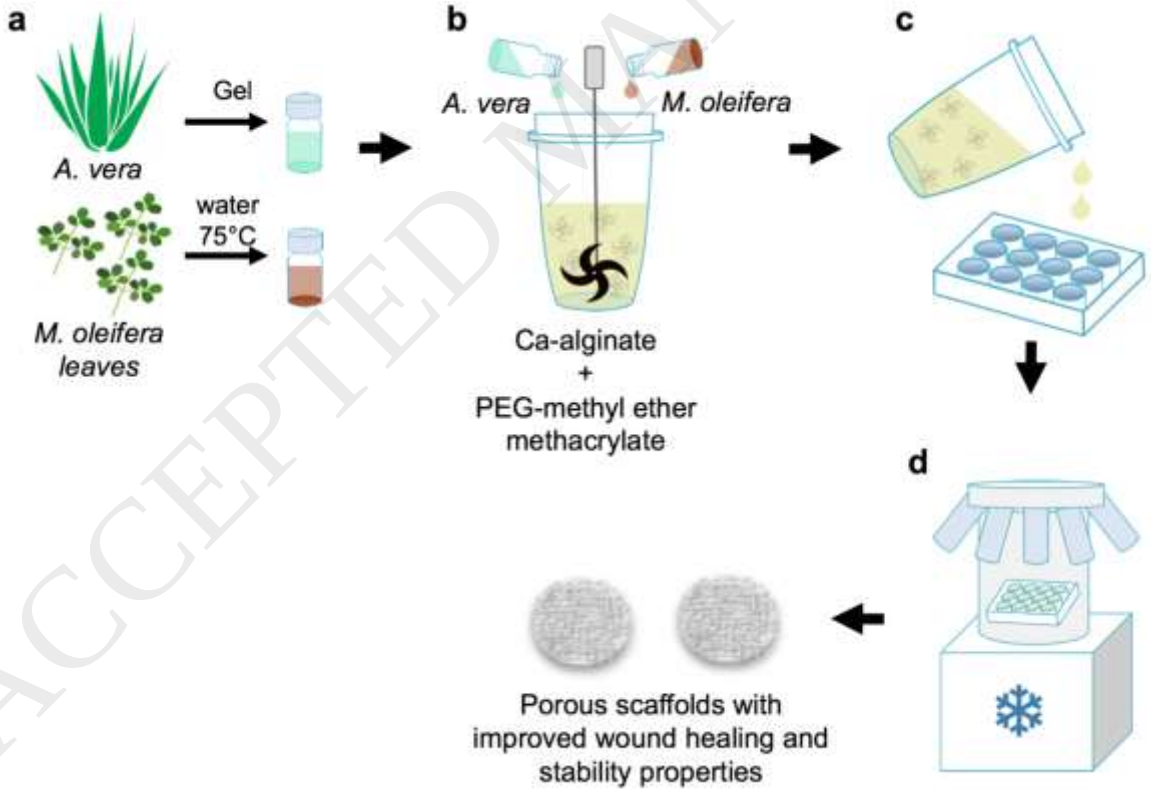


**Fig. 1**. Schematic representation of the preparation process of composite scaffolds. (a) *A. vera* gel was cut from the inner part of the leaves and concentrated by freeze-drying. Phytochemical compounds from *M. oleifera* leaves were extracted by water at 75 °C for 5 min, and concentrated by freeze-drying. (b) *M. oleifera* and/or *A. vera* extracts were homogenized with alginate, $CaCl_2$ and PEG-methyl ether methacrylate

(PEGMA) using a stick blender (c). The alginate-PEGMA-extracts were poured into polystyrene molds and frozen at -4 °C for 48 h, and then (d) freeze-dried for 24 h to obtain porous scaffolds with improved wound healing and stability properties.

### 2.4. Spectroscopic and microscopic characterization

The structure of the surface and cross sections of scaffolds were imaged using scanning electron microscopy (SEM) EVO/MA15 ZEISS at a voltage of 15 kV, under variable pressure conditions. The chemical composition of the scaffolds was analyzed in a FT-IR spectrophotometer (Agilent Cary 630, ATR cell) in the range from 600 to 4000 $cm^{-1}$. Superficial diffractograms were recorded in a D8 ADVANCE Micro-diffractometer (Bruker, Germany) with Cu Kα radiation (λ = 1.5406 Å) from 5° to 70°, using a step scan mode with the step of 0.01° (2θ), 2 s per step with a spot dimension of 0.3 mm. X-ray tube voltage and current were set at 40 kV and 40 mA, respectively.

### 2.5. Non-targeted metabolomic analysis of scaffolds

To further analyze the phytochemical compounds (metabolites) present in the scaffolds, we employed liquid chromatography coupled to high-resolution mass spectrometry (LC-HR-MS) using an Eksigent nanoLC® 400 system (AB Sciex, Foster City, CA, USA) with a HALO Phenyl Hexyl column (0.5 x 50 mm, 2.7 μm, 90 Å pore size, Eksigent AB Sciex, Foster City, CA, USA) interfaced with a TripleTOF 5600+ mass spectrometer (AB Sciex, Foster City, CA, USA). For details of the method, please refer to **supplementary methods**. Before LC-HR-MS analysis, each scaffold (1.5 x 3 $mm^2$) was placed on a vial with 0.5 ml ethyl acetate and 0.5 ml acetone, stirred for 1 min and then sonicated for 10 min in an ice bath. Samples were centrifuged at 18,000 x *g* for 10 min at 4° C, and the supernatant transferred to a previously weighed Eppendorf® tube. The extracted compounds were concentrated using a SpeedVac® at 22 °C for 1.5 h. The concentrated extracts were kept at -80 °C until LC-HR-MS analysis.

### 2.6. Handling, stability and water uptake properties

Handling properties were evaluated by comparing the shape, in terms of the scaffolds diameter, before and after being completely bent. For this, unplasticized and plasticized scaffolds were placed inside open plastic tweezers and then, tweezers were closed until the tip of each lever were in contact with each other. After this, tweezers were open and the scaffolds were taken out from the tweezers and their shape was compared.

Scaffolds stability was evaluated in terms of their integrity and shape retention as a function of immersion time (0, 23, 86, 94, and 110 h) in phosphate-buffered saline (PBS) 1X at 37 °C, with occasional agitation. The PBS solution was not refreshed throughout this assay to avoid scaffolds crumbling, due to samples manipulation.

Water uptake was measured based on the sample weights after absorption in distilled water. Each scaffold (15 mm diameter x 3 mm high) was fully soaked in distilled water (2 ml) for 30, 60, 90, and 120 min, at 37 °C. After absorption, the swollen samples were removed. The excess moisture from the scaffolds surface was absorbed with delicate task wipers. A triplicate set of

samples was analyzed for each composite scaffold. Water uptake was calculated using the following formula:

$$\text{Water uptake, \%} = \frac{M_t - M_0}{M_0} \times 100$$

where $M_t$ is the mass of the scaffold at time = t and $M_0$ is the initial mass of the scaffold.

2.7. Colorimetric quantifications

Each scaffold (15 x 3 $mm^2$) was soaked in 2 ml of distilled water at 37 °C. The distilled water was refreshed after 30, 60, 90, and 120 min. The refreshed water was saved at 4 °C for total phenolic content, antioxidant capacity and anti-inflammatory activity (related to NO scavenging) assays. All the assays were done in triplicate. The methods for each evaluation are described next.

2.7.1. Determination of total phenolic content

The Folin-Ciocalteu method (Singleton, Orthofer & Lamuela-Raventós, 1999) was used to determine the total phenolic content, with the following modifications: 100 μl of 0.2 N Folin-Ciocalteu and 20 μl of sample were transferred to a 96-well plate and mixed thoroughly. After 5 min, 80 μl of 700 mM $Na_2CO_3$ were added and incubated in darkness at 22°C. After 2 hours, the absorbance was measured at 760 nm against a water blank (BioTek Epoch plate reader). Gallic acid was used as a standard (0 – 125 μg/ml) and results were expressed as nmol of gallic acid equivalent per 10 mg of scaffold.

2.7.2. Determination of antioxidant activity

The antioxidant capacity was examined by the DPPH assay (Skotti, Anastasaki, Kanellou, Polissiou & Tarantilis, 2014) with some modifications: the DPPH radical ($DPPH^{\bullet}$) solution (60 μM) was prepared in absolute ethanol. A volume of 150 μl of 60 μM DPPH and 50 μl of sample were mixed in a 96-well plate and incubated at 22°C in darkness for 30 min, thereafter the absorbance was recorded at 517 nm. The percentage of absorbance inhibition at 517 nm was calculated using the formula:

$$\text{Inhibition, \%} = \frac{Abs_{control} - Abs_{sample}}{Abs_{control}} \times 100$$

where $Abs_{control}$ and $Abs_{sample}$ are absorbance values of the control and the sample at 30 min, respectively.

A standard curve was obtained by using a standard solution of Trolox at different concentrations (0 – 100 nmol/ml) in absolute ethanol. The $DPPH^{\bullet}$ inhibition, or scavenging effects of extracts contained in the composite scaffolds, was compared to that of the Trolox standard, and the results

were expressed in terms of nmol Trolox equivalent antioxidant capacity (TEAC) per 10 mg of scaffold.

2.7.3. Anti-inflammatory activity related to NO scavenging

The sodium nitroprusside (SNP) assay was used to determine the NO scavenging capacity of the extracts contained in the composite scaffolds. A volume of 80 μl of 5 mM SNP and 20 μl of sample were mixed in a 96-well plate and incubated in darkness at 22°C. After 60 min, 100 μl of 1X Griess Reagent was added to the wells and incubated in darkness at 22°C. Absorbance at 540 nm was read after 15 min. The NO scavenging was determined using the next formula:

$$\text{NO scavenging, \%} = \frac{Abs_{control} - Abs_{sample}}{Abs_{control}} \times 100$$

where $Abs_{control}$ is the absorbance of Griess Reagent with SNP and $Abs_{sample}$ is the absorbance of Griess Reagent with SNP and sample (Kavoosi & Amirghofran, 2017; Pardau, Pereira, Apostolides, Serem & Bester, 2017).

2.8. Antimicrobial activity

The antimicrobial activity of the composite scaffolds was evaluated by modification of the agar disk diffusion method. The composite scaffolds (15 mm diameter x 3 mm high) were placed on LB agar plates, and then 10 ml of LB agar containing either $1x10^6$ CFU $mL^{-1}$ of *S. aureus* or $0.5x10^6$ CFU $mL^{-1}$ of *E. coli*, were evenly spread over agar plates. Carbenicillin® (30 μl of a 500 μg/ml solution) was used as positive control in 6 mm Whatman® disks. Plates were incubated at 37 °C for 12 h for *S. aureus* and 6 h for *E. coli*. The antibacterial effects of the composite scaffolds were evaluated by comparing the sizes of the inhibitions zones diameters (Liu et al., 2018).

2.9. Cell viability assay

Human skin fibroblasts CCD-1112SK cells were cultured to 80% confluence in Iscove's Modified Dulbecco's Medium (IMDM) supplemented with 10% fetal bovine serum (FBS) and 1% of antibiotic/antimycotic solution in humidified atmosphere with 5% $CO_2$ at 37°C. Cells were detached from the plate using 1ml of trypsin and incubated for 5 min at 37°C. The solution with cells was centrifuged at 800 x *g* for 5 min. The collected cells were counted using a Neubauer chamber with trypan blue (0.4%, Sigma-Aldrich).

Scaffolds were placed (in triplicate) on 24-well plates and $3x10^5$ cells were seeded per well with IMDM supplemented medium. The plates were then incubated in a humidified atmosphere with 5% $CO_2$ at 37°C. Growth medium was replaced every 48 h.

Scaffolds were incubated for 3, 6, and 10 days. Thereafter, the unattached cells on the composite scaffolds were washed with PBS 1X (pH 7.4). The cells adhered onto the scaffolds, and those that remained attached to the wells periphery, were detached by trypsin and then transferred to a 96-well plate. Finally, 20 μl of MTS was added and plates incubated for 4 h. Absorbance was measured at 450 nm (BioTek Epoch plate).

2.10. Statistical analysis of data

Results on the phenolic content, antioxidant capacity, NO scavenging , and antimicrobial activity were statistically analyzed by one way ANOVA, while cell viability was analyzed by two way ANOVA using Tukey's *a posteriori* test. Differences were considered statistically significant for $p<0.05$. Statistical analysis were performed using GraphPad Prism 7.0 software. Three specimens were used for the evaluation of each composite scaffold.

## 3. Results and discussion

3.1. Effect of PEGMA on Ca-alginate scaffolds

To study the interactions between alginate and PEGMA, FT-IR spectroscopy was performed on unplasticized and plasticized alginate-based scaffolds. In the alginate spectrum the peak at 3208 $cm^{-1}$ is assigned to the stretching vibration of O-H bonds. The peaks at 1593 and 1404 $cm^{-1}$ represent the asymmetric and symmetric stretching vibrations of the $COO^-$ group, respectively. The peaks at 1078 and 1021 $cm^{-1}$ are attributed to the stretching vibration of the C-O-C bond (Gao, Pollet & Avérous, 2017) (**Fig. 2a**). The PEGMA spectrum presents a characteristic band at 2868 $cm^{-1}$, corresponding to the C-H stretching of the $-CH_3$ group. The peak at 1717 $cm^{-1}$ is attributed to the C=O stretching of the carbonyl group (Zhang et al., 2012) (**Fig. 2a**). The unplasticized and plasticized Ca-alginate scaffolds showed similar FT-IR patterns as the alginate powder. But for PEGMA plasticized Ca-alginate scaffolds, the peaks at 1593 and 1404 $cm^{-1}$, representing the asymmetric and symmetric stretching vibrations of the $COO^-$ group, respectively, shifted towards higher frequencies. Generally, a weakened bond will shift to lower frequencies. A plausible explanation for the opposite results is that the original hydrogen bonds between water and alginate are weakened due to the intercalation of large amount of water and plasticizer. PEGMA is hydrophilic, then the band at 1593 $cm^{-1}$ shifted to higher frequencies. These suggests that the hydrogen bonds between alginate and water were partially replaced by the relatively weaker hydrogen bonds between PEGMA-alginate at the same time (Gao, Pollet & Avérous, 2017; Ping, Nguyen, Chen, Zhou & Ding, 2001). The appearance of the C=O band at 1717 $cm^{-1}$ in the FT-IR spectrum of Ca-alginate-PEGMA scaffold confirms the composite formation (Laurienzo, Malinconico, Motta & Vicinanza, 2005). The intensity of the band at 2868 $cm^{-1}$, corresponding to the C-H stretching, increased in the plasticized scaffold as a result of the increasing of C-H groups provided by PEGMA.

Diffraction analysis was used to determine the crystalline structures of alginate powder, unplasticized and plasticized alginate scaffolds and PEGMA for comparison purpose (**Fig. 2b**). Sodium alginate powder showed main diffractions peaks at $2\theta$ of 13.8°, 22.3° and 38.4°, which correspond to the (100), (200) and the third related to the amorphous nature of sodium alginate (Thakur & Arotiba, 2018). The peak at $2\theta$ of 13.8° became broader and its intensity increased in the plasticized scaffold compared with the unplasticized, which indicates that there was a reduction in the degree of crystallinity due to plasticization of PEGMA, leading to a more amorphous structure. The crystalline peak of PEGMA was not detected in the plasticized alginate scaffold (**Fig. 2c**), suggesting that PEGMA does not recrystallize in the alginate matrix. Therefore, PEGMA can intercalate between alginate chains disrupting the original alginate structure.

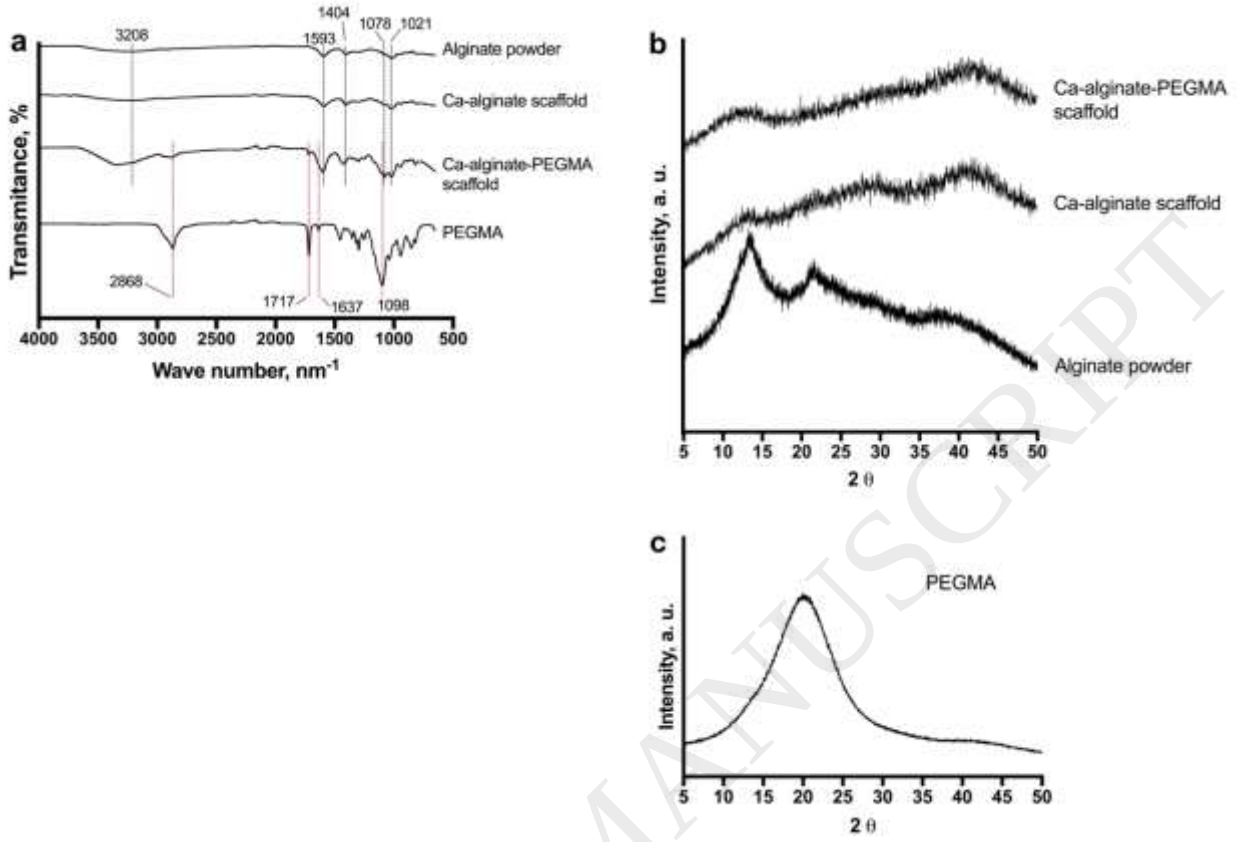


**Fig. 2**. Effect of PEGMA on Ca-alginate scaffolds. (**a**) FT-IR spectra and (**b**) X-ray diffraction patterns of the different alginate-based scaffolds and (**c**) PEGMA.

In the present study, we prepared spongious alginate-based wound dressings of 15 mm diameter x 3 mm high, to which PEGMA has been incorporated to reduce the intermolecular attraction forces between the alginate chain, and thus improving the handling and stability properties of the alginate-based materials. In our alginate scaffolds, plasticization is been done to a certain degree that allowed us to keep the porous three-dimensional structure required for tissue scaffolding applications. Thus, our materials are porous and flexible, but not as elastic as an alginate-plasticized film.

A scaffold should have sufficient mechanical integrity to allow handling during implantation, and also during the remodeling process after implanted (Basu, 2017; O'Brien, 2011). The improved handling properties of the plasticized scaffolds were apparent after being completely bent. **Fig 3a** shows the shape retention in terms of the scaffold diameter, suggesting that the plasticized scaffolds can be handled during implantation without significantly affecting their shape.

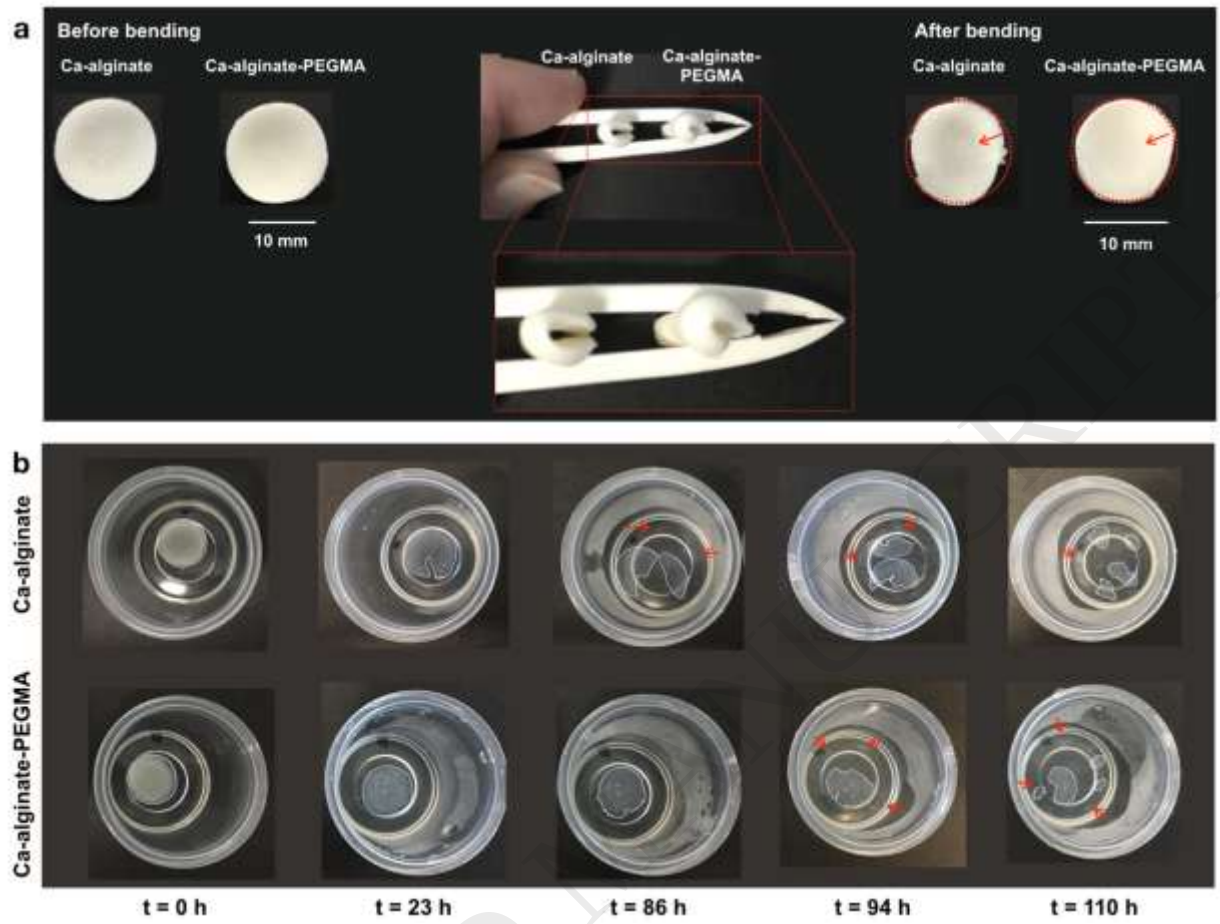


**Fig. 3**. Effect of PEGMA on (**a**) the handling, shape retention and (**b**) stability to aqueous medium of the alginate scaffolds. The blue arrows point to the bent segment of the scaffolds. The red arrows point to small pieces of the disintegrated scaffolds. The shape of the scaffolds was delineated with a red dotted line to show the scaffolds shape retention in terms of its diameter and, a white continuous line to show the shape changes throughout the time.

For tissue engineering applications, scaffolds are expected to degrade during wound healing. Therefore, we studied the effect of PEGMA on the stability of the unplasticized and plasticized alginate-based scaffolds. During the first 23 h of the assay, the Ca-alginate scaffolds began to disintegrate. Before 86 h, the scaffold split in two segments. Compared with unplasticized, Ca-alginate-PEGMA scaffold showed a delayed disintegration (**Fig. 3b**). This result is attributed to the incorporation of PEGMA on alginate. Polymer degradation is mainly controlled by polymer chemistry and physical features of a scaffold (Li, Cooper Jr., Mauck & Tuan, 2006). Diffraction analysis showed that PEGMA can intercalate between alginate chains, leading to a more amorphous structure. In general, hydrophilic or amorphous polymers show increased degradability, in an aqueous medium, than hydrophobic or crystalline polymers. Both alginate and PEGMA are hydrophilic polymers, however the methyl and methacrylate hydrophobic groups present in PEGMA (Jones et al., 2005), make this polymer less hydrophilic than alginate, thus Ca-alginate-PEGMA scaffolds showed a delayed degradation compared with pure alginate-based

scaffolds. Based on this, Ca-alginate scaffolds plasticized with PEGMA showed an increased stability to aqueous medium.

3.2. Structural characteristics and chemical composition of composite scaffolds

The microstructure of the surface (**Fig. 4a-d**) and cross sections (**Fig. 4a'-d'**) of the scaffolds was analyzed by Scanning Electron Microscopy, SEM. These biocomposites are intended to be applied as three-dimensional structures that provide support for tissue formation, thus an interconnected pore structure is of critical importance (O'Brian, 2011). All of our scaffolds had semispherical and interconnected pores between 50 – 100 μm in both, surface and cross sections (**Fig. 4a-d, a'-d'**). The adequate range of pore sizes for any scaffold depends on the cell type used and the tissue to be implanted on (O'Brien, 2011). For human skin fibroblast cell growth, pores smaller than 160 nm are suitable (Yang et al., 2002). Thus, our scaffolds comply with that architecture requisite. Although SEM does not provide quantitative information about porosity, it can be seen that pores distribution is quite similar for all of the scaffolds, independently if a plant extract was or not incorporated (**Fig. 4a-d, a'-d'**). This indicates that the extracts have been added without significantly affecting the architecture of the scaffolds.

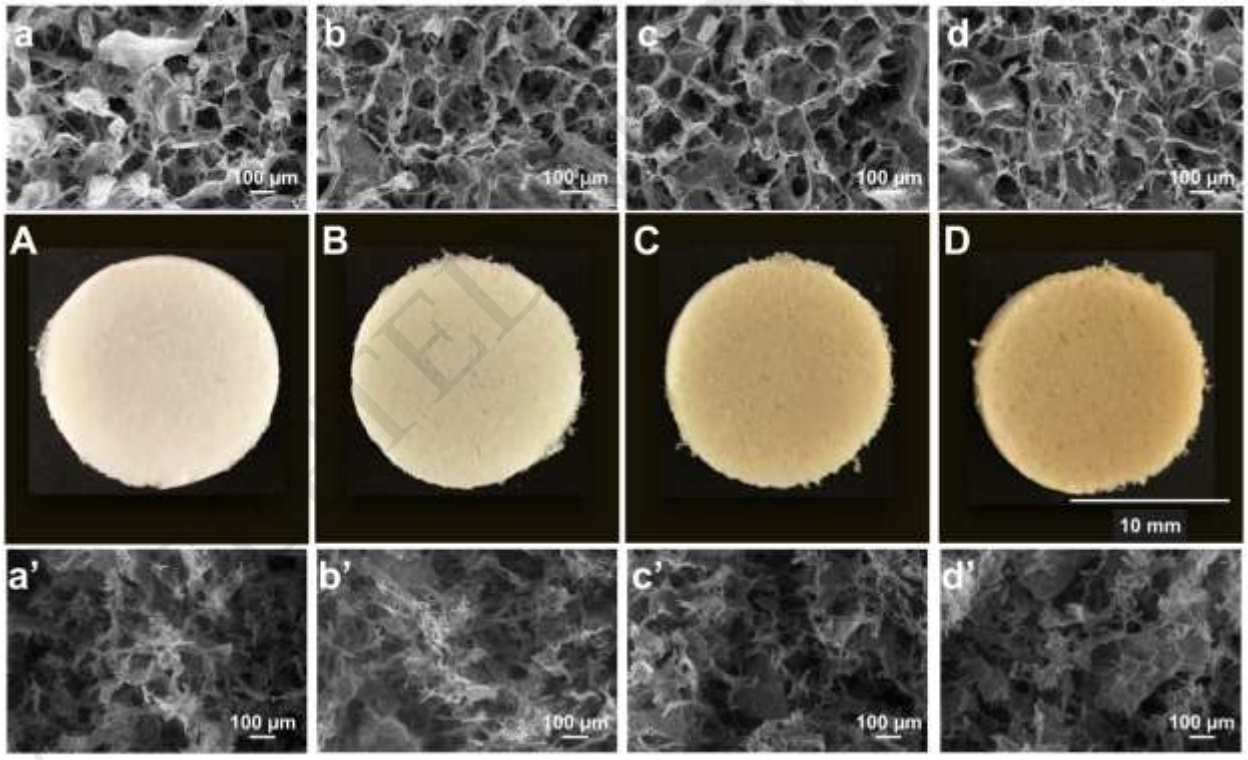


**Fig. 4**. Photographs of representative scaffolds. SEM micrographs show the microstructure of the surface (**a – d**) and cross (**a' – d'**) sections of (**a, a'**) Ca-alginate-PEGMA scaffold, blended with (**b, b'**) 1% (w/v) *A. vera*, or (**c, c'**) 1% (w/v) *A. vera* – 1% (w/v) *M. oleifera*, or (**d, d'**) 1% (w/v) *A. vera* – 2% (w/v) *M. oleifera*.

The composition of biocomposite scaffolds would influence water uptake and release of phytochemicals (derived from plant extracts) when implanted into wounded tissue. Metabolomic analysis by means of LC-HR-MS is a powerful technique that allows to obtain a snapshot of

dozens to hundreds of metabolites or compounds present in natural products extracts. Therefore, to assess for phytochemicals present in extracts and potentially associated with the biological effects of scaffolds on cultured cells, we performed a non-targeted metabolomic analysis by employing LC-HR-MS and online database searching (i.e. METLIN and Global Natural Products Social Molecular Networking [GNPS]). As metabolomic studies by LC-HR-MS often comprises the generation of data containing hundreds to thousands of variables or peaks related to compounds, proper data analysis is necessary to reduce the complexity of omics data. All details of metabolomics data processing are described in **Supporting information.** The total ion chromatograms (TIC) of representative samples are shown in **Supplementary Fig. 1.** The tight clustering of quality control (QC) samples in the principal component analysis (PCA) indicates a reliable assurance of the LC-HR-MS method employed (**Supplementary Fig. 2**). Spectral data searching in online databases of processed data by appropriate software, described in **Supporting information,** indicate the presence of aloin A, aloeresin A, roseoside and aloenin metabolites in AV composite scaffolds (**Table 1**). On the other hand, AV–MO biocomposites, in addition to the above mentioned metabolites, were positive to the presence of quercetin and

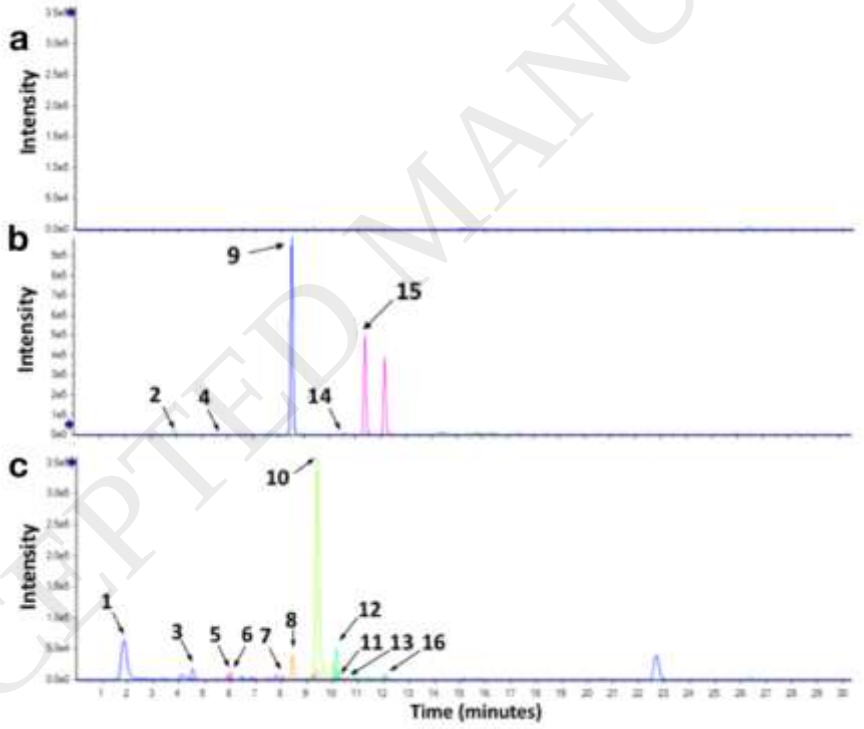


**Fig. 5**. Representative extracted ion chromatograms (EICs) of potential metabolites identified in scaffolds. (**a**) EIC of alginate-PEGMA scaffolds, without extracts. (**b**) EIC of 395.1361 (2), 387.2026 (4), 411.1290 (9), 541.1717 (14) and 419.1350 (15) m/z signals in *A. vera* composite scaffold. (**c**) EICs of 355. 1029 (1), 369.1186 (3), 521.2021 (5), 595.1662 (6), 611.1609 (7), 303.0504 (8), 551.1044 (10), 317.0654 (11), 479.1194 (12), 523.2174 (13), and 491.118 (16) m/z signals in *A. vera* – *M. oleifera* composite scaffolds obtained under positive ionization mode. Numbers of peaks refers to compounds tentatively identified in **Table 1**.

**Table 1**. Differential metabolites identified by LC-HR-MS in *Aloe vera* (AV) and *Aloe vera* - *Moringa oleifera* (AV-MO) composite scaffolds

| Peak | RT (min) | $[M+H]^+$ (accurate mass) | $MS^2$ fragment ions (m/z) | Putative metabolite | Mass accuracy (ppm) |
|---|---|---|---|---|---|
| | | | **AV-MO composite scaffolds** | | |
| **1** | 1.87 | 355.1029 | 266.9959, 163.0391, 145.0285, 73.0479 | Chlorogenic acid | 1.40 |
| **2** | 3.84 | 395.1361 | 377.1233, 359.1135, 329.1028, 299.0920, 275.0918, 257.0808, 245.0807, 233.0810, 203.0697 | 7-hydroxy-5-methyl-2-(2-oxopropyl)-8-[3,4,5-trihydroxy-6-(hydroxymethyl)oxan-2-yl]chromen-4-one | 1.6 |
| **3** | 4.5 | 369.1186 | 177.0547, 149.0595, 145.0283, 134.0374, 117.0332 | 3-Feruloylquinic acid | 1.6 |
| **4** | 5.5 | 387.2026 | 225.1506, 207.1374, 189.1259, 161.1315, 149.0960, 135.1160, 123.0798, 95.0858 | Roseoside | 1.7 |
| **5** | 5.87 | 521.2021 | 323.1296, 311.1292, 291.1028, 219.1019, 217.0862, 189.0905, 175.0756, 137.0595 | 2-(hydroxymethyl)-6-[4-[(2S,3S)-3-(hydroxymethyl)-5-[(E)-3-hydroxyprop-1-enyl]-7-methoxy-2,3-dihydro-1-benzofuran-2-yl]-2-methoxyphenoxy]oxane-3,4,5-triol | 2.3 |
| **6** | 5.99 | 595.1662 | 287.0561 | Kaempferol 3-O-rutinoside | 0.84 |
| **7** | 8.05 | 611.1609 | 303.0504 | Rutin | 0.32 |
| **8** | 8.43 | 303.0504 | 285.0414, 257.0443, 229.0483, 165.0179, 137.0229 | Quercetin | 1.64 |
| **9** | 8.44 | 411.1279 | 249.0757, 207.0656, 151.0391 | Aloenin | -3.16 |
| **10** | 9.39 | 551.1044 | 303.0506 | 3-[[(2R,3S,4S,5R,6S)-6-[2-(3,4-dihydroxyphenyl)-5,7-dihydroxy-4-oxochromen-3-yl]oxy-3,4,5-trihydroxyoxan-2-yl]methoxy]-3-oxopropanoic acid | 1.27 |
| **11** | 10.16 | 317.0654 | 302.0424, 285.0387, 274.0462 | 3-O-Methyl quercetin (isorhamnetin) | -0.63 |
| **12** | 10.16 | 479.1194 | 317.0672, 302.0438 | Isorhamnetin 3-O-glucoside | 2.08 |
| **13** | 10.20 | 523.2174 | 237.1115, 219.1017, 201.0907, 189.0908, 174.0679 | (+)-Isolariciresinol monoglucoside | -0.1 |
| **14** | 10.60 | 541.1717 | 421.1298, 395.1353, 377.1239, 329.1024, 299.0930, 275.0919, 257.0815, 245.0818, 147.0439 | Aloeresin A | 1.9 |
| **15** | 11.40 | 419.1350 | 257.0815, 239.0703, 211.0752 | Aloin A | 3.10 |
| **16** | 12.02 | 491.118 | 287.0548, 187.0597, 127.0385 | Kaempferol 3-O-acetyl-glucoside | 2.60 |
| | | | **AV composite scaffolds** | | |
| **2** | 3.84 | 395.1361 | 377.1233, 359.1135, 329.1028, 299.0920, 275.0918, 257.0808, 245.0807, 233.0810, 203.0697 | 7-hydroxy-5-methyl-2-(2-oxopropyl)-8-[3,4,5-trihydroxy-6-(hydroxymethyl)oxan-2-yl]chromen-4-one | 1.6 |
| **4** | 5.5 | 387.2026 | 225.1506, 207.1374, 189.1259, 161.1315, 149.0960, 135.1160, 123.0798, 95.0858 | Roseoside | 1.7 |
| **9** | 8.43 | 411.1290 | 249.0766, 207.0652, 151.0390 | Aloenin | -0.48 |
| **14** | 10.60 | 541.1717 | 421.1298, 395.1353, 377.1239, 329.1024, 299.0930, 275.0919, 257.0815, 245.0818, 147.0439 | Aloeresin A | 1.9 |
| **15** | 11.38 | 419.1350 | 257.0816, 239.0701, 211.0757 | Aloin A | 3.10 |

kaempferol derivatives, as well as chlorogenic acid and other polyphenols, all of them previously reported in *M. oleifera* extracts. No metabolites were identified in extracted ion chromatograms (EICs) of blank (alginate-PEGMA scaffolds) (**Fig.5a-c**, **Table 1**). Aloin A is one of the active ingredients in *Aloe vera* gel and it has been previously demonstrated that aloin can promote a faster rate of wound closure (Li et al., 2017). Chlorogenic acid is a hydrophilic polyphenol that has protective effect on skin against UV-induced oxidative damage, possibly due to the reduction of ROS (Kitagawa, Yoshii, Morita & Teraoka, 2011). Polyphenols derivatives such as rutin and its metabolite quercetin are known for their antiulcer behavior *in vivo* (Lauro, Torre, Maggi, De Simone, Conte & Aquino, 2002), also by their anti-inflammatory action. A previous study showed that rutin and quercetin exert anti-inflammatory action in 2,4,6-trinitrobenzene sulfonic acid (TNBS)-induced colitis of rats (Kim et al., 2005). The polyphenolic compounds identified on scaffolds by LC-HR-MS come from water extracts from *M. oleifera* and *A. vera* gel, that were blended with alginate-PEGMA to form the composite scaffolds. Although quercetin is less hydrophilic, rutin, chlorogenic acid and aloin A are hydrophilic polyphenols. Thus, their releasement and availability to cells is expected, once placed in contact with the physiological medium of a wounded tissue.

3.3. Physicochemical properties

Cell adhesion and proliferation in scaffolds are facilitated by high water uptake, hydrophilicity and interconnectivity of a porous architecture (Depan, Girase, Shah & Misra, 2011). In scaffolds for wound healing applications, a good water uptake indicates that the material can absorb the wound exudate, which helps to form a moist healing environment (Chen et al., 2018). Scaffolds based on alginate-PEGMA (blank scaffolds) and those blended with *A. vera* (AV-composite scaffolds), had the highest water absorption, 1515±114% and 1512±132%, respectively (**Fig. 6a**). However, the hydration capacity of the scaffolds reduced to 1172±69% and 918±26%, for those containing 1% (w/v) *M. oleifera* or 2% (w/v) *M. oleifera*, respectively (**Fig. 6a**). The water uptake capability of a biomaterial depends mainly on the hydrophilicity and porosity of the materials (Sultana & Hayat Khan, 2013). SEM analysis showed that the microstructure and porosity of the scaffolds are quite similar between them, independently of their composition (**Fig. 4**). The porosity of the scaffolds could also be related to the crosslinking degree in the alginate-PEGMA-extracts biocomposites but, all of the scaffolds had the same $Ca^{2+}$ and PEGMA concentrations. Thus, the difference in the water uptake profiles between our scaffolds may be related to the hydrophilicity of the incorporated extracts. LC-HR-MS indicates that quercetin, a relatively hydrophobic metabolite (Kitagawa et al., 2011), is contained in the *M. oleifera* scaffolds (**Fig. 5c**, **Table 1**). Thus, water uptake profile was influenced by the composition of the scaffolds and the porous morphology that all of the scaffolds exhibited, as indicated by SEM (**Fig. 4**). The porous morphology could facilitate the entrapment of water in the scaffolds matrix (Kumar Ramadas et al., 2014). In addition, the incorporation of *A. vera* could contribute to increase in water uptake because of its water absorbing property (Li et al., 2017). The water uptake capacity of our scaffolds is similar to other alginate composite dressings for hemostasis applications (1200 – 1400% swelling degree) (Cheng et al., 2017), or scaffolds made of konjac glucomannan-keratin biopolymers with *Avena sativa* (1000% water absorption) for diabetic wound healing (Veerasubramanian et al., 2018).

Phenolic compounds were extracted by water and then blended with alginate-PEGMA polymeric matrix, therefore these phenolic compounds are expected to be solubilized into the aqueous medium of a wounded tissue. Thus, we evaluated the rate of solubilization of extracts by measuring the increment of phenolics in the water in contact with scaffolds by the Folin-Ciocalteu assay. Solubilization rate profile mainly depended on the type of extract, rather than its concentration (**Fig. 6**). For example, the phenolic compounds from 1% (w/v) *A. vera* (AV composite) are released more rapidly than those from the AV-MO composite scaffolds. However, *A. vera–M. oleifera* and *A. vera*–2% (w/v) *M. oleifera* blends from AV-MO composite and AV-2MO composite, respectively, are released at similar rates (**Fig. 6b**). When comparing the water uptake and extracts release profiles, we can see that AV composite scaffolds absorbed more water than those with AV-MO and AV-2MO while, at the same time, the AV biocomposite had a larger burst effect than the other scaffolds. Incorporation of *M. oleifera* slower the release rate of phenolic compounds, mainly because of the less hydrophilic character of some components in *M. oleifera* extract, such as quercetin (**Fig. 5c**, **Table 1**). These results are in agreement with previous reports on the release profile of bioactive compounds from alginate-hyaluronan composites, where the 70% of Trenaxamic acid was released during the first 30 min. In this case, addition of hyaluronan accelerated the release rate, given its hydrophilic property which caused a faster water absorption with a consequent larger burst effect (Catanzano et al., 2017). Moreover, the solubilization rate results demonstrated that the plant extracts were homogeneously distributed throughout the scaffolds, allowing the phytochemical components of the plant extracts being part of the alginate-PEGMA matrix. This was one of our goals since, as previously mention, *A. vera* and *M. oleifera* contain phytochemical compounds that promote fibroblasts adhesion (Chin, Jalil, Ng & Ng, 2018; Li et al., 2017), a lacking property in pure alginate scaffolds.

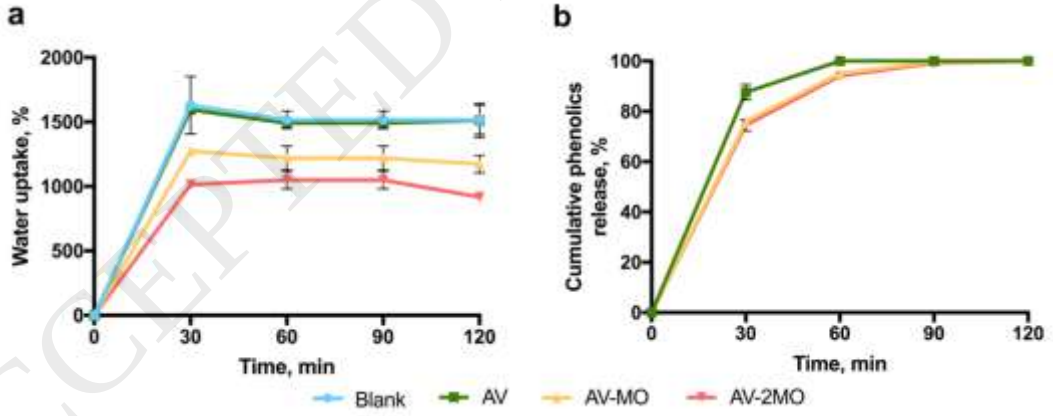


**Fig. 6**. (**a**) Water uptake of scaffolds. (**b**) Rate of solubilization of extracts-derived phenolic compounds into aqueous medium. **Blank**: Alginate-PEGMA scaffold. **AV**: Alginate-PEGMA-1% (w/v) *A. vera* scaffold. **AV-MO**: Alginate-PEGMA-1% (w/v) *A. vera*-1% (w/v) *M. oleifera* scaffold. **AV-2MO**: Alginate-PEGMA-1% (w/v) *A. vera*-2% *M. oleifera* scaffold. Error bars show one standard deviation (n = 3/group).

### 3.3. Phenolic content, antioxidant and anti-inflammatory activities

Total phenolic content in composite scaffolds was determined by the Folin-Ciocalteu colorimetric assay, and expressed as nmol of gallic acid equivalent per 10 mg of scaffold. AV composite scaffolds had the lowest phenolic content, 16.13±2.0 nmol GAE/10 mg scaffold, while

incorporation of *M. oleifera* into the alginate-PEGMA-AV blend, increased the total phenolic content to 203.4±4.4 nmol GAE/10 mg scaffold, i.e. 12.7 times higher ($p$<0.0001) with respect to AV biocomposites. Doubling the concentration of *M. oleifera* from 1% (w/v) to 2% (w/v) increased total phenolics to 287.9±8.5 nmol GAE/10 mg scaffold, i.e. 1.4 times higher ($p$<0.0001) with respect to AV-MO composites, and 18 times higher ($p$<0.0001) with respect to AV composite scaffolds (**Fig. 7a**).

Antioxidant activity was determined by the DPPH$^{\bullet}$ method and expressed as nmol Trolox equivalent antioxidant capacity per 10 mg of scaffold. The effects of extracts towards DPPH$^{\bullet}$ radicals indicates the presence of compounds with the ability to interact towards free radicals by acting as an electron donor or hydrogen atoms (Skotti et al., 2014). Antioxidant activity increased from 22.28±0.87 nmol TEAC/10 mg scaffold in AV composite materials, to 175.36±2.66 nmol TEAC/10 mg scaffold for AV-MO biocomposites, i.e. 7.9 times ($p$<0.0001) and, to 207.56±5.1 nmol TEAC/10 mg scaffold for AV-2MO composite scaffolds, i.e. 9.3 and 1.2 times ($p$<0.0001), with respect to AV and AV-MO biocomposites, correspondingly (**Fig. 7b**). Thus, the higher the phenolic content, the greater the antioxidant effect of the prepared composite scaffolds. This is in agreement with previous works that indicate that the total phenolic content is a major contributor to the antioxidant activity, for some herbs (Skotti et al., 2014; Zhang et al, 2011). During wound healing, both neutrophils and macrophages produce reactive oxygen species, ROS, as a defense mechanism against invading microbes. However, excessive ROS production leads to oxidative stress that can have detrimental effects on wound healing. In chronic, non-healing wounds, high levels of ROS have been associated with impaired wound repair (Dunnill et al., 2017; Schafer & Werner, 2008). A previous study showed that a 0.01% (w/v) *M. oleifera* leaves extract, with an antioxidant activity (measured as $EC_{50}$) of 62.94 μg/ml, significantly reduced the relative amount of intracellular ROS from 540 to 408%, in HEK-293 cells (Vongsak et al., 2013). Although we used higher concentrations of *M. oleifer*a to prepare our scaffolds, the antioxidant capacity of our *M. oleifera* extract had a $EC_{50}$ of 300 μg/ml (results not shown), which means that we needed to use higher extract concentration to scavenge the 50% of the free radicals from DPPH$^{\bullet}$. Based on this, the antioxidant capabilities of our composite scaffolds are expected to enhance wound healing by reducing ROS to adequate levels to support wound healing.

The anti-inflammatory activity of composite scaffolds was evaluated in terms of their ability to scavenge nitric oxide, NO, a pro-inflammatory mediator that when released at high levels during pathological conditions triggers inflammation (Sharma, Al-Omran & Parvathy, 2007). The NO scavenging activity of the biocomposites was determined with the sodium nitroprusside, SNP, assay. NO produced by SPN reacts with Griess reagent to produce a pink-red color complex, which is disrupted in presence of NO scavengers (Kavoosi & Amirghofran, 2017; Pardau et al., 2017). Therefore, the lower the absorbance at 540 nm, the greater the NO scavenging and thus, the higher anti-inflammatory activity related to NO removal capacity of the composite scaffolds. All of our biocomposites have NO scavenging activity (**Fig. 7c**). Blank, i.e. alginate-PEGMA scaffolds, scavenged NO by 17.88%. These scaffolds do not contain extracts, however it has been previously reported that PEG possesses anti-inflammatory properties (Ackland et al., 2010). Thus, NO scavenging capacity of scaffolds without extracts could be attributed to the incorporation of PEGMA. Addition of *A. vera* to composite scaffolds did not influence NO scavenging capacity of the biocomposites, since no statistical differences were found ($p$>0.05). However, incorporation of 2% (w/v) *M. oleifera* increased NO scavenging of the composite

materials to 30%. *M. oleifera* metabolites, such as quercetin and rutin, have been reported as anti-inflammatory polyphenols (Kim et al., 2005) which is in agreement with the NO scavenging activity found for AV–MO composite scaffolds. Moreover, in a study comparing the anti-inflammatory effects of aloin, a metabolite identified in AV biocomposites (**Fig 5b**, **Table 1**),

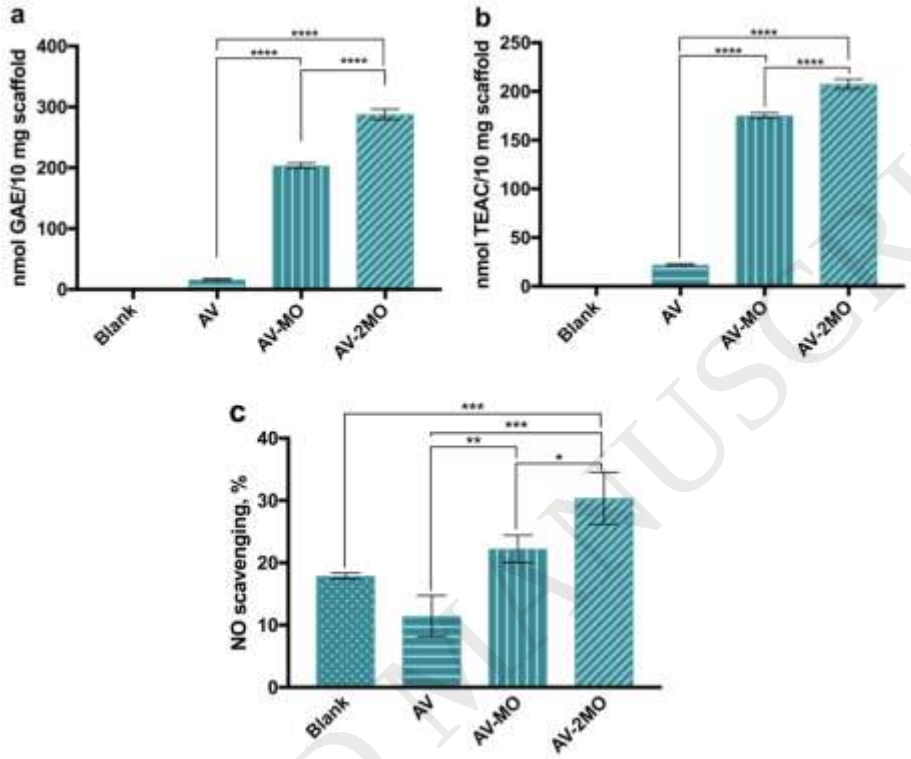


**Fig. 7**. (**a**) Phenolic content of scaffolds, expressed as nmol of gallic acid equivalent (GAE) per 10 mg of scaffold. (**b**) Antioxidant activity, expressed as nmol Trolox equivalent antioxidant capacity (TEAC) per 10 mg of scaffold. (c) Anti-inflammatory activity of scaffolds related to NO scavenging. **AV-MO**: Alginate-PEGMA-1% (w/v) *A. vera*-1% (w/v) *M. oleifera* scaffold. **AV-2MO**: Alginate-PEGMA-1% (w/v) *A. vera*-2% (w/v) *M. oleifera* scaffold. Error bars show one standard deviation (n = 3/group). The level of significance is denoted as * ($p$<0.05), ** ($p$<0.01), *** ($p$<0.001) and, **** ($p$<0.0001).

aloe-emodin, genistein, daidzein, kaemferol and quercetin, also identified in our scaffolds with *M. oleifera* (**Fig 5c**, **Table 1**), aloin showed the lowest anti-inflammatory effect, while quercetin showed the highest effect (Park, Kwon & Sung, 2009), which is in agreement with our results. In addition, other studies have reported a correlation between the anti-inflammatory activity and total phenolic content of medicinal plants (Pardau, Pereira, Apostolides, Serem & Bester, 2017; Zhang et al., 2011). Although we did not perform a correlation analysis, we found that the scaffolds with higher anti-inflammatory activity were those with higher phenolic content (**Fig. 7**). Thus, our results are in agreement with previous findings. Compounds with anti-inflammatory properties can accelerate wound healing, in part because of reduction of neutrophil infiltration and inhibition of production of tumor necrosis factor alpha (TNF-$\alpha$) by inflammatory cells (Shimizu, Watanabe, Arawaka, Fujiwara, Higuchi & Kuroki, 2000). Thus, the anti-inflammatory activity of our scaffolds would enhance wound healing by contributing to modulate the inflammatory response.

3.5. Antimicrobial activity

The antimicrobial effect of composite scaffolds was evaluated against representative Gram-positive strain, *Staphylococcus aureus*, and Gram-negative strain, *Escherichia coli*, which are prevalent in infectious wounds (**Fig. 8**). Neither blank scaffolds, i.e. alginate-PEGMA, nor AV composite scaffolds exhibited activity against any of the bacterial strains that we evaluated. A previous study compared the antibacterial activity of aqueous, ethanol and acetone extracts of *A. vera* against *S. aureus*, *Streptococcus pyogens*, *Pseudomonas aeruginosa* and *E. coli*. Only

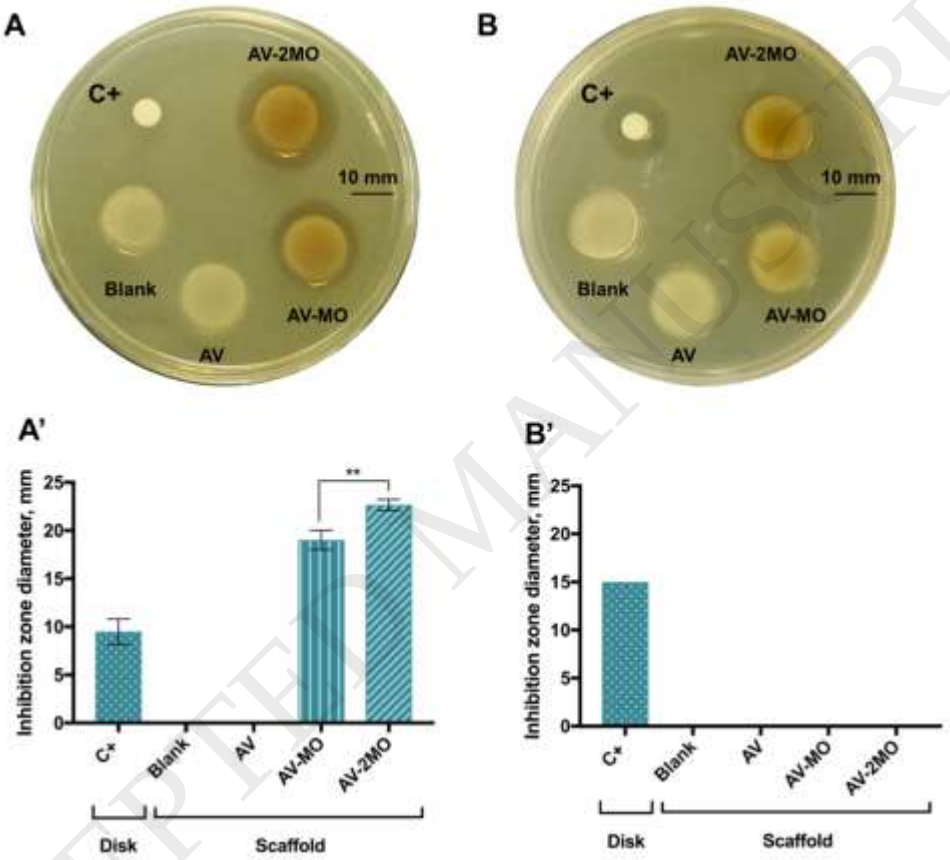


**Fig. 8**. Antimicrobial activity of the scaffolds. (**A**) Photographs showing the inhibition zones of AV–MO and AV-2MO composite scaffolds against *Staphylococcus aureus* after 12 h of incubation, at 37 °C. (**A'**) Diameter of the inhibition zones of the scaffolds against *S. aureus*. (**B, B'**) Biocomposites did not show antimicrobial activity against *E. coli* after 6 h of incubation at 37 °C. **C+**: Antibiotic disk with Carbenicillin®, as positive control. **Blank**: Alginate-PEGMA scaffold. **AV**: Alginate-PEGMA-1% (w/v) *A. vera* scaffold. **AV-MO**: Alginate-PEGMA-1% (w/v) *A. vera*-1% (w/v) *M. oleifera* scaffold. **AV-2MO**: Alginate-PEGMA-1% (w/v) *A. vera*-2% *M. oleifera* scaffold. Error bars show one standard deviation (n = 3/group). The level of significance is denoted as ** ($p$<0.01).

ethanol and acetone extracts showed activity against *S. aureus* and *E. coli*. The aqueous extract only showed activity against *S. pyogens* (Arunkumar & Muthuselvam, 2009). We used the water-soluble fraction of the inner gel of *A. vera* to prepare the composite scaffolds, therefore our results are in agreement with previous reports on null antimicrobial activity of aqueous extracts of *A. vera* against *S. aureus* and *E. coli* (Arunkumar & Muthuselvam, 2009). However, AV-MO composite

scaffolds showed activity against *S. aureus*, but not *E. coli*. Moreover, increasing the concentration of *M. oleifera*, from 1 to 2% (w/v) in AV-2MO, increased the antibacterial effect of composite materials, i.e. the diameter of the inhibition zone was larger ($p$<0.001) (**Fig. 8A, B**). Therefore, antibacterial activity of our materials was attributed to the incorporation of *M. oleifera* extracts into the composite scaffolds. Previous studies have correlated phenolic content and antioxidant capacity with antimicrobial activity (Grabek-Lejko, Słowik & Kasprzyk, 2018; Peixoto et al., 2018; Vázquez-Armenta et al., 2017). Doubling the concentration of *M. oleifera* incorporated into composite scaffolds increased phenolics and antioxidant activity (**Fig. 7a-b**). Thus, the higher antimicrobial activity found in AV-2MO compared with AV-MO can be attributed to the higher phenolic content and antioxidant activity of the composite scaffolds. A proposed explanation for the antibacterial properties of polyphenols compounds is that these compounds can form soluble complexes with proteins and bind to bacterial adhesins. By doing so, polyphenols disturb the signaling of receptors on the cell surface (Brantner & Grein, 1994) which finally inhibits the growth of bacteria. On the other hand, *S. aureus* is one of the dominant Gram-positive organisms involved in the initial stage of the infectious process after a skin injury occurs, while Gram-negative *E. coli* is found in later stages, i.e. when a chronic wound is developed (Cardona & Wilson, 2015). Therefore, the antimicrobial activity of *M. oleifera*-containing scaffolds would complement tissue healing by inhibiting the growth of *S. aureus,* one of the Gram-positive organisms found in early-stage of the infectious process.

3.6. Cell viability

Cell viability was analyzed by the MTS assay by seeding CCD-1112Sk human skin fibroblasts onto scaffolds for 10 days. Any increase or decrease in viable cell number can be detected by measuring formazan concentration reflected in optical density (OD) (van Meerloo, Kaspers & Cloos, 2011) at 450 nm and, for our analysis, directly relate it to the viability of cells seeded on the composite scaffolds. With respect to incubation time, addition of blended *A. vera–M. oleifera* to alginate-PEGMA increased viability of the cells in the composite scaffolds at the 3$^{rd}$ day of evaluation, compared with scaffolds that did not contain extracts or contain only *A. vera* ($p$<0.05). After 10 days of incubation, all of the composite scaffolds containing extracts of *M. oleifera* and/or *A. vera*, showed higher cell viability compared with scaffolds without extracts ($p$<0.05). With respect to each type of scaffold, the fibroblasts viability was influenced by the type and concentration of the extract blended with alginate-PEGMA. For blank, i.e. alginate-PEGMA scaffolds, fibroblasts viability did not increase ($p$>0.05) from days 3 to 10. However, when *A. vera* was incorporated into the scaffolds, more fibroblasts remained viable as the incubation time increased from 3 to 10 days and the same behavior was found for AV-MO composite scaffolds (**Fig. 9**). However, doubling the concentration of *M. oleifera* did not increase cell viability in AV-2MO composite scaffolds with respect to AV-MO materials ($p$>0.05). It has been proposed that the amount of water associated with the scaffolds plays a crucial role in cell attachment and proliferation (Depan et al., 2011). Our results on water uptake behavior showed that AV-2MO scaffolds absorbed less water than AV-MO biocomposites (**Fig. 6a**). Thus, a plausible explanation for such finding is that the reduced water uptake noted with 2% (w/v) *M. oleifera* extract could be correlated with the lower cell proliferation found. Cells distribute over a confluent layer due to a meshwork or bundles of actin-containing microfilaments that permit the movement of penetrating

cells along a substratum (Siebers, ter Brugge, Walboomers & Jansen, 2005; Wang & van Blitterswijk, 2010), and the water associated with the scaffolds directly affects the growth of this cell layer (Depan et al, 2011). If AV-2MO scaffolds absorbed less water, the continuous cell layer formed over time onto the scaffolds (results not shown) could be washed away. Thus, our results show that fibroblasts viability increased ($p$<0.05) when *A. vera* or the blend 1% (w/v) *A. vera*-1% (w/v) *M. oleifera* were used to prepare the alginate-PEGMA scaffolds. Aloin, a metabolite identified in our AV composite scaffolds (**Fig. 5b, Table 1**), is an anthraquinone compound that is highly stable and has excellent water solubility. A previous work demonstrated that aloin can directly promote the proliferation of fibroblasts and vascular endothelial cells (Li et al., 2017). Moreover, for *M. oleifera*, is been reported that aqueous leaf extracts promote proliferation of human dermal fibroblasts (Chin et al., 2018). Therefore, our results are in agreement with previous findings, since scaffolds containing *M. oleifera* and/or *A. vera* showed higher cell viability than pure alginate-PEGMA scaffolds. Summarizing, incorporation of *A. vera* and *M. oleifera*, each at 1% (w/v), increased the cell number in alginate-based scaffolds, which is of prime importance in biomaterials for tissue scaffolding applications.

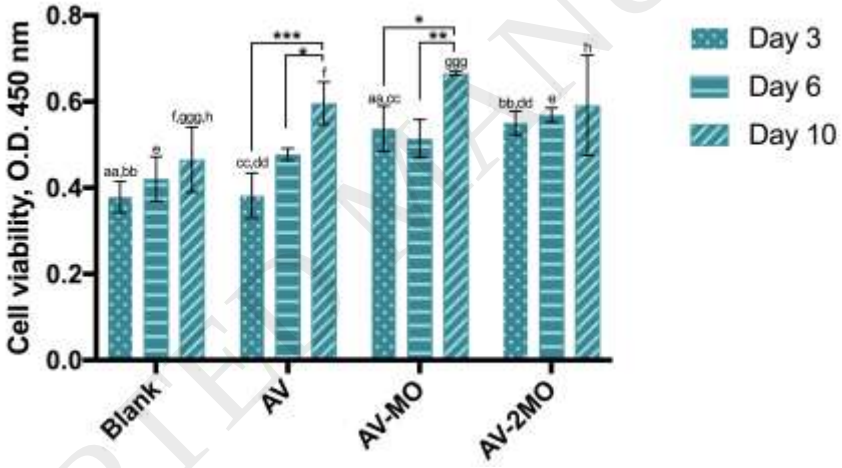


**Fig. 9**. Viability of human skin fibroblast (CCD-1112Sk cells) on scaffolds. **Blank**: Alginate-PEGMA scaffold. **AV**: Alginate-PEGMA-1% (w/v) *A. vera* scaffold. **AV-MO**: Alginate-PEGMA-1% (w/v) *A. vera*-1% (w/v) *M. oleifera* scaffold. **AV-2MO**: Alginate-PEGMA-1% (w/v) *A. vera*-2% (w/v) *M. oleifera* scaffold. Error bars show one standard deviation (n = 3/group). Asterisks indicate statistical differences between days of evaluation of cell viability for the same type of composite scaffold. The level of significance is denoted as * ($p$<0.05), ** ($p$<0.01) and, *** ($p$<0.001). Letters indicate statistical differences between types of scaffolds at the same day of evaluation. The level of significance is denoted as e,f,h ($p$<0.05), aa,bb,cc,dd ($p$<0.01) and, ggg ($p$<0.001).

## 4. Conclusions

Scaffolds based on alginate-PEGMA and *M. oleifera* and/or *A. vera* were prepared and evaluated in cell-free and cell-based assays. A delayed disintegration and increased stability to aqueous medium were obtained when alginate was plasticized with PEGMA. This plasticization

was optimized to the point of increasing the handling and stability to aqueous medium, while keeping a porous architecture which is required for tissue scaffolding applications.

*A. vera* contributed to increase the water uptake capability of the scaffolds, due to its high water absorbing property. While *M. oleifera* provided antioxidant capacity, improved anti-inflammatory properties (related to NO scavenging) and imparted antimicrobial activity against *S. aureus*, to the alginate-PEGMA-based scaffolds. These healing properties were mainly attributed to the polyphenolic compounds contained in these plants, since antioxidant, anti-inflammatory and antimicrobial capacities increased as the phenolic content in the scaffolds was higher. Blending 1% (w/v) *A. vera* and 1% (w/v) *M. oleifera* with Ca-alginate-PEGMA, produced scaffolds that significantly increased, after 10 days of evaluation, the number of viable human skin fibroblasts cells, compared with Ca-alginate-PEGMA scaffolds without plant extracts. These results were attributed to the active components present in *A. vera* gel and *M. oleifera* leaves aqueous extracts. These characteristics make alginate-PEGMA-*A. vera*-*M. oleifera* scaffolds a good choice for further evaluations (such as *in vivo* wound healing studies) for wound healing applications.

## Conflict of interest

The authors declare no conflict of interest.

## Acknowledgements

The Complementary Support Program from Cátedras-Consejo Nacional de Ciencia y Tecnología (Cátedras-CONACyT) (No. 266145; 2015) is acknowledged. We thank Luis Gradilla from Ciencias de la Tierra, CICESE, for helping with SEM imaging. Eber Daniel Villa-Rodríguez, Cindy Manríquez-Rodríguez and Fernando Díaz-Castillo are also thanked for their valuable technical help pertaining the preparation of samples for LC-HR-MS and software analysis. Dr. Enrique Íñiguez-Pacheco, from Centro Mexicano de Innovación en Energía Geotérmica (CeMIEGeo), is acknowledged for helping with XRD. The enthusiastic participation of Sujey López-Celis, from Instituto Tecnológico de Tijuana, during preliminary experiments of this work, is gratefully appreciated.

## Appendix A. Supplementary data

LC-HR-MS methods, data processing and analysis, total ion chromatograms (TICs) of representative scaffolds, and Principal Component Analysis (PCA) and Principal Component Variable Grouping (PCVG) of biomaterial samples.

**References**

Ackland, G.L., Gutierrez Del Arroyo, A., Yao, S.T., Stephens, R.C., Dyson, A., Klein, N.J., Singer, M. & Gourine, A.V. (2010). Low-molecular weight polyethylene glycol improves survival in experimental sepsis. *Critical Care Medicine*, *38*(2), 629-636.

Arunkumar, S. & Muthuselvam, M. (2009). Analysis of phytochemical and antimicrobial activities of *Aloe vera* L. against clinical pathogens. *World Journal of Agricultural Sciences*, *5*(5), 572-576.

Augst, A.D., Kong, H.J. & Mooney, D.J. (2006). Alginate hydrogels as biomaterials. *Macromolecular Bioscience*, *6*, 623-633.

Basu, B. (2017). Biomaterials for musculoskeletal regeneration. Concepts. Springer Nature. DOI: 10.1007/978-981-10-3059-8.

Brantner, A. & Grein, E. (1994). Antibacterial activity of plant extracts used externally in traditional medicine. *Journal of Ethnopharmacology*, *44*, 35-40.

Cardona, A.F. & Wilson, S.E. (2015). Skin and soft-tissue infections: a critical review and the role of telavancin in their treatment. *Clinical Infectious Diseases*, *61*(S2), S69-S78.

Catanzano, O., D'Esposito, V., Formisano, P., Boateng, J.S. & Quaglia, F. (2018). Composite alginate-hyaluronan sponges for the delivery of tranexamic acid in postextractive alveolar wounds. *Journal of Pharmaceutical Sciences*, *107*(2), 654-661.

Chanda, A., Adhikari, J., Ghosh, A., Chowdhury, S.R., Thomas, S., Datta, P. & Saha, P. (2018). Electrospun chitosan/polycaprolactone-hyaluronic acid bilayer scaffold for potential wound healing applications. *International Journal of Biological Macromolecules*, *116*, 774-785.

Chen, H., Lan, G., Ran, L., Xiao, Y., Yu, K., Lu, B., Dai, F., Wu, D. & Lu, F. (2018). A novel wound dressing based on Konjac glucomannan/silver nanoparticle composite sponge effectively kills bacteria and accelerates wound healing. *Carbohydrate Polymers*, *183*, 70-80.

Cheng, F., Lui, C., Wei, X., Yan, T., Li, H., He, J. & Huang, Y. (2017). Preparation and characterization of 2,2,6,6,-tetramethylpiperidine-1-oxyl (TEMPO)-oxidized cellulose nanocrystal/alginate biodegradable composite dressing for hemostasis applications. *ACS Sustainable Chemistry & Engineering*, *5*(5), 3819-3828.

Chin, C.-Y., Jalil, J., Ng, P.Y. & Ng, S.-F. (2018). Development and formulation of *Moringa oleifera* standardized leaf extract film dressing for wound healing application. *Journal of Ethnopharmacology*, *212*, 188-199.

Depan, D., Girase, B., Shah, J.S. & Misra, R.D.K. (2011). Structure-process-property relationship of the polar graphene oxide-mediated cellular response and stimulated growth of osteoblasts on hybrid chitosan network structure nanocomposite scaffolds. *Acta Biomaterialia*, *7*, 3432-3445.

Dunnill, C., Patton, T., Brennan, J., Barret, J., Dryden, M., Cooke, J., Leaper, D. & Georgopoulos, N.T. (2017). Reactive oxygen species (ROS) and wound healing: the functional role of ROS and emerging ROS-modulating technologies for augmentation of the healing process. *International Wound Journal*, *14*, 89-96.

Falanga, V. (2005). Wound healing and its impairment in the diabetic foot. *Lancet*, *366*, 1736-1743.

Gao, C., Pollet, E. & Avérous, L. (2017). Innovative plasticized alginate obtained by thermo-mechanical mixing: effect of different biobased polyols systems. *Carbohydrate Polymers*. *157*, 669-676.

Grabek-Lejko, D., Słowik, J. & Kasprzyk, I. (2018). Activity of selected honey types against *Staphylococcus aureus* methicillin susceptible (MSSA) and methicillin resistant (MRSA) bacteria and its correlation with hydrogen peroxide and antioxidant capacity. *Farmacia*, *66*(1), 37-43.

Guo, F., Zhang, H., Qiu, G., Zou, H., Chen, G., Lou, Y., Min, D. & Guo, G. (2018). Fabrication of LaCl3-containing nanofiber scaffolds and their application in skin wound healing. *Journal of Applied Polymer Science*, DOI: 10.1002/APP.46672

Jones, J.A., Novo, N., Flagler, K., Pagnucco, C.D., Carew, S., Cheogn, C., Kong, X.Z., Burke N.A.D. & Stöver H.D.H. (2005). Thermoresponsive copolymers of methacrylic acid and poly(ethylene glycol) methyl ether methacrylate. *Journal of Polymer Science Part A: Polymer Chemistry*, *43*, 6095-6104.

Kavoosi, G. & Amirghofran, Z. (2017). Chemical composition, radical scavenging and anti-oxidant capacity of *Ocimum basilicum* essential oil. *Journal of Essential Oil Research*, *29*(2), 189-199.

Kim, H., Kong, H., Choi, B., Yang, Y., Kim, Y., Lim, M.J., Neckers, L. & Jung, Y. (2005). Metabolic and pharmaceutical properties of rutin, a dietary quercetin glycoside, for treatment of inflammatory bowel disease. *Pharmaceutical Research*, *22*(9), 1499-1509.

Kitagawa, S., Yoshii, K., Morita, S-y. & Teraoka, R. (2011). Efficient topical delivery of chlorogenic acid by an oil-in-water microemulsion to protect skin against UV-induced damage. *Chemical and Pharmaceutical Bulletin*, *59*(6), 793-796.

Kumar Ramadass, S., Perumal, S., Gopinath, A., Nisal, A., Subramanian, S. & Madhan, B. (2014). Sol-gel assisted fabrication of collagen hydrolysate composite scaffold: a novel therapeutic alternative to the traditional collagen scaffold. *ACS Applied Materials & Interfaces*, *6*, 15015-15025.

Laurienzo, P., Malinconico, M., Motta., A. & Vicinanza, A. (2005). Synthesis and characterization of a novel alginate-poly(ethylene glycol) graft copolymer. *Carbohydrate Polymers*, *62*, 274-282.

Lauro, R.M., Torre, M.L., Maggi, L., De Simone, F., Conte, U. & Aquino, R.T. (2002). Fast- and slow-release tablets for oral administration of flavonoids: rutin and quercetin. *Drug development and Industrial Pharmacy*, *28*(4), 371-379.

Li, L.-J., Gao,S.-Q., Peng, L.-H., Wang, X.-R., Zhang, Y., Hu, Z.-J. & Gao, J.Q. (2017). Evaluation of aloin in treating acute trauma in vitro and in vivo. *Biomedicine & Pharmacotherapy*, *88*, 1211-1219.

Li, W.-J., Cooper Jr.. J.A., Mauck, R.L. & Tuan, R.S. (2006). Fabrication and characterization of six electrospun poly($\alpha$-hydroxy ester)-based fibrous scaffolds for tissue engineering applications. *Acta Biomaterialia*, *2*, 377-385.

Liu, J., Xiao, J., Li, F., Shi, Y., Li, D. & Huang, Q. (2018). Chitosan-sodium alginate nanoparticle as a delivery system for $\varepsilon$-polylysine: preparation, characterization and antimicrobial activity. *Food Control*, *91*, 302-310.

O'Brien, F.J. (2011). Biomaterials & scaffolds for tissue engineering. *Materials Today*, *14*(3), 88-95.

Park, M-Y., Kwon, H-J., & Sung, MK. (2009). Evaluation of aloin and aloe-emodin as anti-inflammatory agents in aloe by using murine macrophages. *Bioscience, Biotechnology, and Biochemistry*, *73*(4), 828-832.

Pardau, M.D., Pereira, A.S.P., Apostolides, Z., Serem, J.C. & Bester, M.J. (2017). Antioxidant and anti-inflammatory properties of *Ilex guayusa* tea preparations: a comparison to *Camellia sinensis* teas.

Partap, S., Lyons, F. & F.J. O'Brien. (2010). Scaffolds & Surfaces. In: Basic engineering for medics and biologists. An ESEM Primer. Lee, T.C. & P.F. Niederer (Eds.) IOS Press, *152*, 187.

Peixoto, C.M., Dias, M.I., Alves, M.J., Calhelha, R.C., Barros, L., Pinho, S.P. & Ferreira, I.C.F.R. (2018). Grape pomace as a source of phenolic compounds and diverse bioactive properties. *Food Chemistry*, *253*, 132-138.

Pereira, R., Carvalho, A., Vaz, D.C.,Gil, M.H., Mendes, A. & Bártolo, P. (2013). Development of novel alginate based hydrogel films for wound healing applications. *International Journal of Biological Macromolecules*, *52*, 221-230.

Ping, Z.H., Nguyen, Q.T., Chen, S.M., Zhou, J.Q. & Ding, Y.D. (2001). States of water in different hydrophilic polymers – DSC and FTIR studies. *Polymers*, *42*(20), 8461-8467.

Ranjan Saha, N., Roy, I., Sarkar, G., Bhattacharyya, A., Das, R., Rana, D., Banerjee, R., Kanti Paul, A., Mishra, R. & Chattopadhyay, D. (2018). Development of active packaging material based on cellulose acetate butyrate/polyethylene glycol/aryl ammonium cation modified clay. *Carbohydrate Polymers*, *187*, 8-18.

Sarhan, W.A., Azzazy, H.M.E. & El-Sherbiny, I.M. (2016). Honey/chitosan nanofiber wound dressing enriched with *Allium sativum* and *Cleome droserifolia*: enhanced antimicrobial and wound healing activity. *ACS Applied Materials & Interfaces*, *8*, 6379-6390.

Sarkar, R., Ghosh, A., Barui, A. & Datta, P. (2018). Repositing honey incorporated electrospun nanofiber membranes to provide anti-oxidant, anti-bacterial and anti-inflammatory microenvironment for wound regeneration. *Journal of Materials Science: Materials in Medicine*, *29*:31.

Schafer, M. & Werner, S. (2008). Oxidative stress in normal and impaired wound repair. *Pharmacological Research*, *58*, 165-171.

Shah, A. & Amini-Nik, S. (2017). The role of phytochemicals in the inflammatory phase of wound healing. International Journal of Molecular Sciences, 18, 1068. DOI: 10.3390/ijms18051068

Shapiro, L. & Cohen, S. (1997). Novel alginate sponges for cell culture and transplantation. *Biomaterials*, *18*, 583-590.

Sharma, J.N., Al-Omran, A. & Parvathy, S.S. (2007). Role of nitric oxide in inflammatory diseases. *Inflammopharmacology*, 15, 252-259.

Shimizu, N., Watanabe, T., Arawaka, T., Fujiwara, Y., Higuchi K. & Kuroki, T. (2000). Pentoxifyline accelerates gastric ulcer healing in rats: roles of tumor necrosis factor alpha and neutrophils during the early phase of ulcer healing. *Digestion*, *61*, 157-164.

Siebers, M.C., ter Brugge, P.J., Walboomers, X.F. & Jansen, J.A. (2005). Integrin as linker proteins between osteoblasts and bone replacing materials. A critical review. *Biomaterials*, *26*, 137-146.

Singleton, V.L., Orthofer, R. & Lamuela-Raventós, R,M. (1999). Analysis of total phenols and other oxidation substrates and antioxidants by means of Folin-Ciocalteu reagent. *Methods in enzymology*, *299*, 152-178.

Skotti, E., Anastasaki, E., Kanellou, G., Polissiou, M. & Tarantilis, P.A. (2014). Total phenolic content, antioxidant activity of aqueous extracts from selected Greek medicinal and aromatic plants. *Industrial Crops and Products*, *53*, 46-54.

Stagnaro, P., Schizzi, I., Utzeri, R., Marsano, E. & Castellano, M. (2018). Alginate-polymethacrylate hybrid hydrogels for potential osteochondral tissue regeneration. *Carbohydrate Polymers*, *185*, 56-62.

Sultana, N. & Hayat Khan, T. (2013). Water absorption and diffusion characteristics of nanohydroxyapatite (nHA) and poly(hydroxybutyrate-co-hydroxyvalerate-) based composite tissue engineering scaffolds and nonporous thin films. *Journal of Nanomaterials*, http://dx.doi.org/10.1155/2013/479109.

Sun, J. & Tan, H. (2013). Alginate-based biomaterials for regenerative medicine applications. Review. *Materials*, *6*, 1285-1309.

Thakur, S. & Arotiba, O.A. (2018). Synthesis, swelling and adsorption studies of a pH-responsive sodium alginate-poly(acrylic acid) superabsorbent hydrogel. *Polymer Bulletin*, *75*, 4587-4606.

van Meerloo, J., Kaspers, J.L. & Cloos, J. (2011). Cell sensitivity assays: the MTT assay. In: Cancer Cell Culture: Methods and Protocols, 2nd Edition. Ian A. Cree (ed.). Methods in Molecular Biology, *731*, Chapter. 20.

Vázquez-Armenta, F.J., Silva-Espinoza, B.A., Cruz-Valenzuela, M.R., González-Aguilar, G.A., Nazzaro, F., Fratianni, F. & Ayala-Zavala, J.F. (2017). Antibacterial and antioxidant properties of grape stem extract applied as disinfectant in fresh leafy vegetables. *Journal of Food Science and Technology*, *54*(10), 3192-3200.

Veerasubramanian, P.K., Thangavel, P., Kannan, R., Chakraborty, S., Rachandran, B., Suguna, L. & Muthuvijayan, V. (2018). An investigation of konjac glucomannan-keratin hydrogel scaffold loaded with *Avena sativa* extracts for diabetic wound healing. *Colloids and Surfaces B: Biointerfaces*, *165*, 92-102.

Vongsak, B., Sithisarn, P., Mangmool, S., Thongpraditchote, S., Wongkrajang, Y. & Gritsanapan, W. (2013). Maximizing total phenolics, total flavonoids contents and antioxidant activity of *Moringa oleifera* leaf extract by the appropriate extraction method. *Industrial Crops and Products*, *44*, 566-571.

Wang, H. & van Blitterswijk, C.A. (2010). The role of three-dimensional polymeric scaffold configuration on the uniformity of connective tissue formation by adipose stromal cells. *Biomaterials*, *31*, 4322-4329.

Yang, J., Shi, G., Bei, J., Wang, S., Cao, Y., Shang, Q., Yang, G. & Wang, W. (2002). Fabrication and surface modification of microporous poly(L-lactic acid) and poly(L-lactic-*co*-glycolic acid) (70/30) cell scaffolds for human skin fibroblasts cell culture. *Journal of Biomedical Materials Research, 62*, 438-446.

Zhang, L., Ravipati, A.S., Koyyalamudi, S.R., Jeong, S.C., Reddy, N., Smith, P.T., Bartlett, J., Shanmugam, K., Münch, G. & Wu, M.J. (2011). Antioxidant and anti-inflammatory activities of selected medicinal plants containing phenolic and flavonoid compounds. *Journal of Agricultural and Food Chemistry*. 59, 12361-12367.

Zhang, X., Fu, C., Feng, L., Ji, Y., Tao, L., Huang, Q., Li, S. & Wei, Y. (2012). PEGylation and polyPEGylation of nanodiamond. *Polymer*, *53*, 3178-3184.

Zhong, S.P., Zhang, Y.Z. & Lim, C.T. (2010). Tissue scaffolds for skin wound healing and dermal reconstruction. Advanced Review. *WIREs Nanomedicine and Nanobiotechnology*, *2*, 510-525.

Zmora, S., Glicklis, R. & Cohen, S. (2002). Tailoring the pore architecture in 3-D alginate scaffolds by controlling the freezing regime during fabrication. *Biomaterials*, *23*, 4087-4094